Graduate School of Pure and Applied Sciences

Development of Cathode, Anode and Crossover Suppression Membrane for Formic Acid Production by Electrochemical CO_2 Reduction
(電気化学的二酸化炭素還元によるギ酸電解合成に向けた カソード、アノード、クロスオーバー抑制膜に関する研究)

Samuel Jeong

Doctoral Program in Applied Physics
Student ID number: 201930093
Doctor of Philosophy in Engineering
Advised by Yoshikazu Ito

1. Introduction

Since the Industrial Revolution, humankind has relied on fossil fuels as a major source of energy. The massive consumption of fossil fuels by power plants and factories has been continuously releasing carbon dioxide (CO_2) into the atmosphere. There is a growing demand for efficient CO_2 utilization technologies that recycle a large amount of CO_2 into useful chemical products such as energy carriers. Countries around the world are developing technologies for CO_2 capture and utilization (CCU) to reduce CO_2 emissions into the atmosphere to zero in the future. Various CCU methods have been proposed, and recently, electrochemical CO_2 conversion technology has been attracting particular attention. This technology uses an electrochemical CO_2 reduction reaction with electricity generated from renewable energy sources, making it possible to synthesize useful compounds without emitting CO_2 into the atmosphere. This technology is expected to be a method to realize a carbon-recycling society and lead to the sustainable development of humankind.

In recent years, the development of electrosynthesis cells by electrochemical CO_2 reduction has been widely studied. In particular, formic acid electrosynthesis is attracting attention because it is liquid at room temperature and pressure, has low toxicity, and high energy density, and is expected to be used as a candidate for future energy carriers. The cell for formic acid electrosynthesis consists of three main elements as shown in **Figure 1**; (1) At the cathode of the cell, the formic acid electrosynthesis reaction occurs by an electrochemical CO_2 reduction reaction (CO_2ER), (2) At the anode, oxygen evolution reaction (OER) occurs in which water is oxidized, (3) Proton exchange membrane, which separates the anode and cathode, transfers protons and causes electrode reactions. As cathode catalysts, indium and tin have been widely studied as catalysts for formic acid electrosynthesis. Previous reports have focused on controlling reaction intermediates and improving Faraday efficiency by structural control, alloying, and surface modification. However, due to the limitation of CO_2 mass transport in the electrolyte, the Faradaic efficiency decreases when the reaction rate is accelerated by applying high potential. Thus, there is a requirement to improve the mass transport to the catalyst surface and to accelerate the rate of formic acid production. Anode catalysts for OER have also been studied for a long time in the field of water electrolysis reactions. There has been a demand for inexpensive non-noble metal catalysts to replace iridium and ruthenium-based noble metal catalysts in recent years.

Due to the harsh oxidation conditions of the OER, the non-noble metal catalyst is easily corroded, and the lack of durability is a problem. Although various studies have been reported, there is a need to develop a durable catalyst to prevent corrosion of the catalyst due to high overpotential. As proton exchange membranes, Nafion-based materials are often used. Although Nafion has high proton conductivity, it causes fuel crossover, which significantly reduces the product correction efficiency. For crossover suppression, using two-dimensional materials such as graphene has been proposed, but the proton conductivity decreases when pure graphene is used. Therefore, there is a demand to develop materials with both high proton conductivity and suppression of crossover.

In this study, cathode/anode catalysts and crossover suppression membrane have been developed in order to achieve a practical formic acid electrosynthesis cell. As a cathode catalyst, polyethylene glycol (PEG) with high CO_2 adsorption capacity was used to overcome the CO_2 transport to the catalyst surface. A composite catalyst consisting of PEG electrodeposited on porous tin was synthesized and evaluated for catalytic performance. The PEG on the Sn surface promotes the adsorption and transfer of CO_2 to the catalyst surface, increasing the formation rate of formate. The anode catalyst has developed the inexpensive and highly active NiMo alloy covered with chemically stable graphene. The encapsulation effect of graphene on OER activity and lifetime was systematically investigated. The graphene encapsulation significantly enhanced the OER activities of the NiMo anodes and provided long electrode lifetimes and performances comparable to those of commercially available anodes. For the proton exchange membrane, novel graphene-based materials were used for suppressing the crossover. By controlling the number of graphene layers with artificially created nano-sized defects, a novel proton exchange membrane achieves both high proton conductivity and formic acid crossover suppression. These developments of the cathode, anode and proton exchange membrane are expected to advance the practical application of cells for the synthesis of formic acid electrolysis at a low cost using abundant resources.

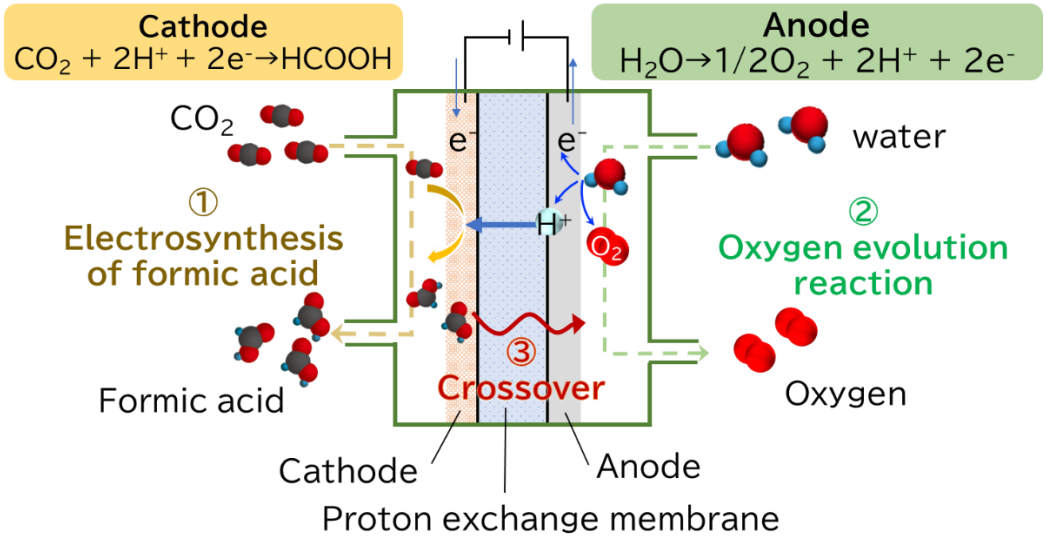

Figure 1. Schematic image of CO_2 electrochemical reduction cell.

2. Experimental

2.1. Material syntheses and device configurations

2.1.1 Preparation of porous Sn sheet

Sn particles were prepared by reducing $SnCl_4$ with $NaBH_4$. The resulting 200-600 nm Sn particles were annealed at a temperature of 250°C for 10 min under a mixed atmosphere of hydrogen and argon gas, leading to the formation of a porous structure.

2.1.2 Preparation of polymer covered porous Sn

The prepared porous Sn sheet as a working electrode was clipped with Ti clip and immersed in an electrolytic solution of KCl with polymer. The graphite rod was used as a counter electrode and Ag/AgCl (sat.) electrode was used as a reference electrode. A direct current of 10 mA cm^{-2} was applied for 1 minute to electrodeposit polymer on the surface. After the electrochemical deposition, the samples were immersed in the Millipore water and washed by exchanging the Millipore water and dried in a vacuum. Polyethylene glycol (PEG) or polyethyleneimine (PEI) was used as the polymer.

2.1.3 Synthesis of porous NiMo alloy

The $NiMoO_4$ nanofibers were synthesized through a standard hydrothermal method.[1, 2] The resulting $NiMoO_4$ nanofibers solution were dropped on Cu sheet as substrates and dried. The dried solution was inserted into a quartz tube furnace and annealed at 950°C for 20 min under the mixed gases of hydrogen and argon to reduce the oxidized precursor to form NiMo alloy with a 3D porous structure.[3] After the furnace cooling down to room temperature, the annealed NiMo samples were peeled off the Cu sheets for further measurements.

2.1.4 Synthesis of NiMo alloy encapsulated by porous graphene

$NiMoO_4$ nanofiber solution was mixed with 18-27 nm SiO_2 nanoparticles. The typical weight ratio of the $NiMoO_4$ nanofibers and SiO_2 nanoparticles is 10^{-3} wt % (SiO_2) for NiMo-Micro hole graphene (i.e., NiMo-MHG), 10^{-4} wt % (SiO_2) for NiMo-Sub Micro hole graphene (i.e., NiMo-SMHG), and 10^{-5} wt % (SiO_2) for NiMo-Nano hole graphene (i.e., NiMo-NHG). After stirring very well, the mixtures were drop-casted on a Cu sheet as substrates and dried completely. The dried mixtures were inserted into the center of a quartz tube furnace and annealed at 950°C for 20 min to grow porous NiMo with the surface containing the SiO_2 nanoparticles under a mixed atmosphere of hydrogen and argon. Then, the temperature was set at 750°C, in which graphene was grown for 1 second under a mixed atmosphere of hydrogen, argon and pyridine. The furnace was immediately opened and the inner quartz tube was cooled down to room temperature with a fan. The samples were separated from the Cu sheets for measurements. For the non-holey graphene samples, NiMo-Fully graphene (i.e., NiMo-FG), the SiO_2 nanoparticles were not mixed with $NiMoO_4$ nanofiber solution and other procedures were made in a similar manner to the NiMo samples encapsulated by holey graphene.

2.1.5 Device configuration for fuel crossover and proton conductivity experiments.

The monolayer pure graphene sheets were prepared on a Cu foil by CVD methods using CH_4 as carbon sources. Nafion film was subsequently coated on the graphene surface as a protective layer through a spin coater. After dissolving Cu foil, the Nafion-protected graphene sheet was transferred onto a Nafion film attached Si_3N_4 chip with a window (size: 20 μm × 20 μm) on the center. Then this chip was employed as separating membranes in an H-type electrolyzer to isolate individual anode and cathode chambers.

2.2. General characterizations

The sample morphology and microstructures were characterized using a scanning electron microscope (SEM), a transmission electron microscope (TEM), X-ray diffraction (XRD). Surface chemical states of samples were

analyzed by X-ray photoelectron spectroscopy (XPS) with Al Ka and X-ray monochromator. Graphene samples were characterized by Raman spectroscopy.

2.3. Electrochemical measurements

The CO_2ER and OER measurements were performed in a three-electrode system, where a-prepared catalyst samples were attached on a glassy carbon rotation disk electrode (RDE), a Au wire or graphite rod, and an Ag/AgCl electrode, served as the working electrode, counter electrode, and reference electrode, respectively. The potential was calculated with respect to reversible hydrogen electrode (RHE) using the equation: E(RHE) = E(Ag/AgCl) + 0.0591*pH + 0.197. The polarization curves were obtained via sweep rate of 50 mV/s for CO_2ER and 5 mV/s for OER measurements. The electrolyte was Ar/CO_2/O_2-saturated, and the RDE rotation speed was 1600 rpm to remove generated carbon monoxide, oxygen or hydrogen bubbles. The electrode potential was automatically *iR*-compensated with the ohmic resistance.

2.4 Determination of formate

Concentrations of formate in the electrolyte solution samples were determined by gas chromatography (GC), equipped with dielectric barrier discharge ionization detector (BID) and Rtx-WAX column (RESTEK Co.), referring to the analysis of formate.

2.5. DFT calculations

The first-principles calculations were performed with the VASP code. The projected augmented wave (PAW) method was used. For the exchange and correlation functional, the Perdew·Burke·Ernzerhof (PBE) functional was used. The plane wave energy cutoff was set to 400 Ry. The dispersion correction was included via the Grimme's D3 (BJ) method. For the estimation of the adsorption energy of CO_2 on the PEG-covered Sn(101) surface were performed the PAW method implemented in the VASP code. PBE functional together with the dispersion correction through the Grimme's D3 (BJ) method was adopted. The density of PEG was modified by inserting one, three, or six PEG chains in the unit cell. The energy barrier for the CO_2 transfer from the PEG chain to the Sn surface for the three PEG chains model was calculated using the nudged elastic band method.

3. Results and Discussions

3.1 Characterizations and CO_2ER performances of PEG covered porous Sn

The morphology of PEG covered porous Sn (PEG/p-Sn) was investigated by SEM measurements. The SEM image exhibited a bicontinuous and interconnected pore structure (**Figure 2a**). The XRD pattern confirmed that the as-synthesized porous NiMo alloy mainly comprises Sn. The thickness of the polymer layers was measured using TEM (**Figure 2b**). The effects of PEG on the porous Sn (p-Sn) surfaces as cathodes were examined by comparing PEG/p-Sn with PEI/p-Sn and p-Sn. Hydrodynamic voltammetry measurements were used to study the electrochemical reduction of CO_2 in Ar- or CO_2-saturated 0.1 M aqueous $KHCO_3$ electrolytes using an Au-wire counter electrode (**Figure 2c**).

The chronoamperometry (CA) tests were performed to determine the Faradaic efficiency (FE) of formate of the various p-Sn cathodes at −1200 mV (vs. RHE) in the CO_2-saturated electrolyte for 6h. Quantitative analysis was performed using NMR by CO_2ER and gas chromatography. The FEs from the average current densities at −1200 mV (vs. RHE) was estimated to be 75% for p-Sn, PEG/p-Sn, and PEI/p-Sn. FEs of the samples at various potentials

were similarly investigated and summarized in **Figure 2d**. The bare p-Sn, which was a benchmark sample, increased the FE from −600 to −700 mV (vs. RHE), while its FE decreased with increasing applied potential. In contrast, the FE of PEG/p-Sn increased at higher applied potentials from −900 to −1200 mV (vs. RHE). The FE of PEI/p-Sn was lower at −900 mV (vs RHE) than the FE of p-Sn and gradually increased as the potential increased but never exceeded the performance of PEG/p-Sn. These results indicate that PEG modification plays an important role in enhancing the selectivity and FE of formate.

The effect of PEG supports on the formation rate of formate was investigated by comparing PEG/p-Sn, PEI/p-Sn, and p-Sn at various potentials (**Figure 2d**). The formation rate in the presence of PEG/p-Sn at a potential of −1200mV is the highest (975 μmol h^{-1} cm^{-2}) among the reported Sn-based catalysts. Thus, the PEG/p-Sn developed in this study can be potentially used for the efficient formation of formate by exploiting the process of CO_2 reduction.

To elucidate the effect of PEG modification on the mechanism of catalysis, the adsorption energy of molecular CO_2 and E_{ads} were calculated by DFT (**Figure 3**). From the calculations, it was found that too thin (one chain) or too thick (six chains) PEG layer was detrimental to the adsorption or transport of CO_2. It was also found that CO_2 adsorption to the polymer and CO_2 transport to the catalyst surface could be enhanced if the thickness of the PEG layer was properly controlled (three chains). Thus, the adsorption of an additional amount of CO_2 on PEG could help eject the adsorbed CO_2 molecules from PEG to the Sn surface.

These experimental and DFT results proposed the following reaction mechanism for the formation of formate on PEG/p-Sn. The PEG/p-Sn demonstrates Faradaic efficiency and a formate formation rate that are 1.3 times and two times higher than those of bare p-Sn at −1200 mV (vs RHE), respectively. This enhancement could be attributed to the cooperative nature of PEG support, a K^+ ion concentration effect[4-7], and complete coverage of the catalysts by the carbon support.

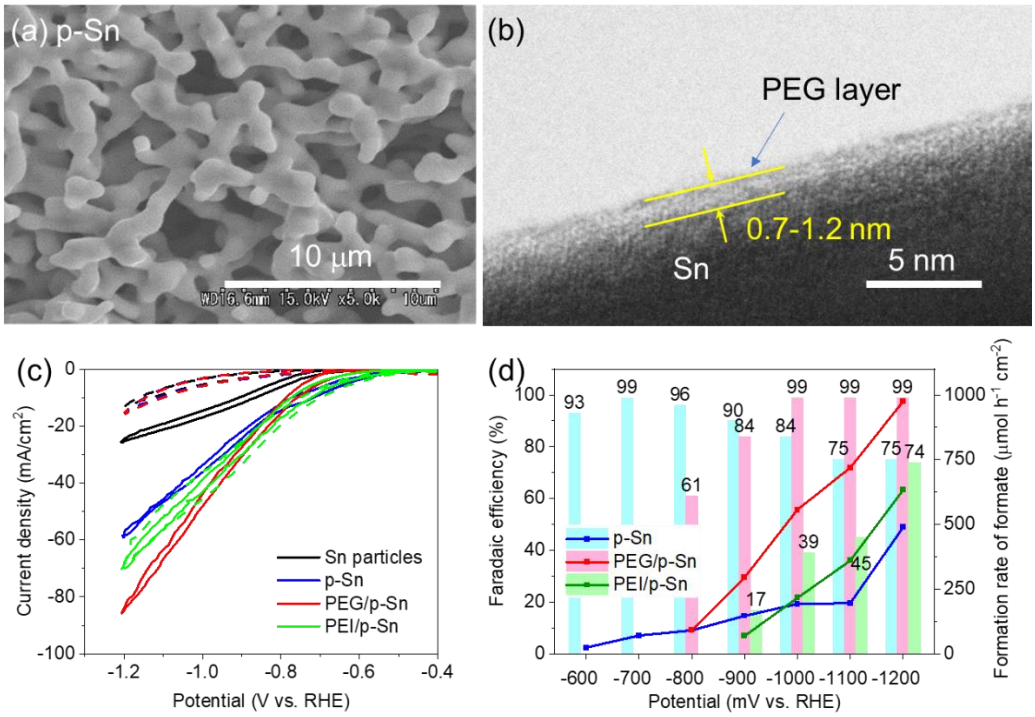

Figure 2 (a) The SEM image of p-Sn. (b) TEM image of PEG/p-Sn. (c) Hydrodynamic voltammograms of various cathodes at 1600 rpm. The dotted and solid lines represent the data in the Ar-saturated electrolyte and CO_2-saturated

electrolyte, respectively. (d) Faradaic efficiencies and formation rates of formate on p-Sn, PEG/p-Sn, and PEI/p-Sn under conditions of varying potential ranges in the CO_2-saturated electrolyte.

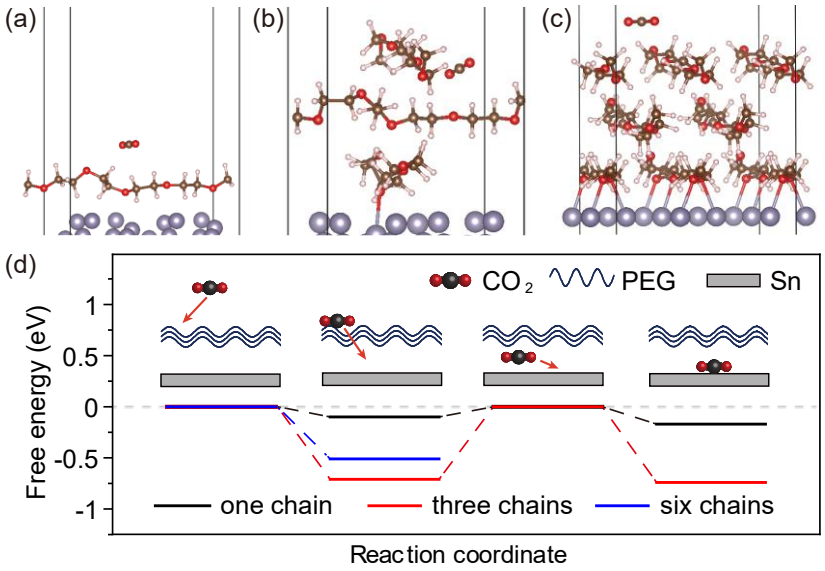

Figure 3. DFT-calculated CO_2 adsorption models for PEG covered Sn. Unit cells of (a) one PEG chain, (b) three PEG chain, and (c) six PEG chain models. (d) Energy diagram of on CO_2 adsorbed on one, three, and six PEG chain models. The inset show a schematic representation of the transition of CO_2 adsorptions on the three PEG chain models. The free energy indicates the total adsorption energy, $E_{tot} - E_{sub} - E_{CO_2}$, where E_{tot} is the total energy of the system, including adsorbed CO_2 molecules, E_{sub} is the energy of the substrate (PEG + Sn), and E_{CO_2} is the energy of CO_2 in the gas phase.

3.2 Characterizations and OER performances of graphene encapsulated porous NiMo alloy

The morphology of graphene encapsulated porous NiMo alloy was investigated by SEM measurements. The SEM image exhibited a bicontinuous and interconnected pore structure (**Figure 4a**). The XRD pattern confirmed that the as-synthesized porous NiMo alloy mainly comprises NiMo. Thus, the materials were characterized as NiMo alloys. The OER catalytic activity of NiMo alloys depending on the graphene coverage from 0 to 100 % was systematically investigated in O_2-saturated 1.0 M KOH electrolyte solution (**Figure 4b**). The OER activities of the NiMo, NiMo-NHG, NiMo-SMHG, and NiMo-MHG anodes were lower than that of NiMo-FG. The overpotential decreased with increasing graphene coverage increased from 0% (NiMo) to <80% (NiMo-MHG), 88% (NiMo-SMHG), >99% (NiMo-NHG), and 100% (NiMo-FG). The performances of NiMo-FG are better than those reported Ni- and Mo-based materials in O_2-saturated 1.0M KOH electrolyte. The effects of graphene encapsulation on the cycling stability of the NiMo anodes were investigated (**Figure 4c**). The OER activity of the bare porous NiMo deposited on a Ni foam (NiMo/NF), and NiMo-SMHG deposited on a Ni foam (NiMo-SMHG/NF) maintained to 59% and 66% after 1000 cycles, respectively. In contrast, NiMo-FG deposited on Ni foam (NiMo-FG/NF) maintained >97% of OER activity after 1000 cycles. These results indicate that the graphene encapsulated samples achieve remarkable stability due to the protection of the sample through graphene encapsulation.

DFT calculations obtained the Gibbs free energy profiles to determine the underlying catalytic mechanism of graphene encapsulation on the NiMo alloy (**Figure 5**). The Gibbs free energies of the OER processes under zero

potential and potential of 1.23 V (vs. RHE) were calculated. The NiMo(100) system demonstrated the highest $|\Delta G_{o*}|$ value, which implies that the bare NiMo surface strongly adsorbs the intermediates through a direct chemical bonding between the metal and O atoms under 1.23 V (vs. RHE). In contrast, graphene/NiMo and N-doped graphene/NiMo showed the low $|\Delta G_{o*}|$ values under 1.23 V (vs. RHE) and graphene encapsulation reduced the adsorption/desorption energy for each reaction step closer to zero. This indicates that the graphene layer on the NiMo surface reduced the free energy difference for the conversion of O* to OOH* species, which is the rate-determining step during the OER process.

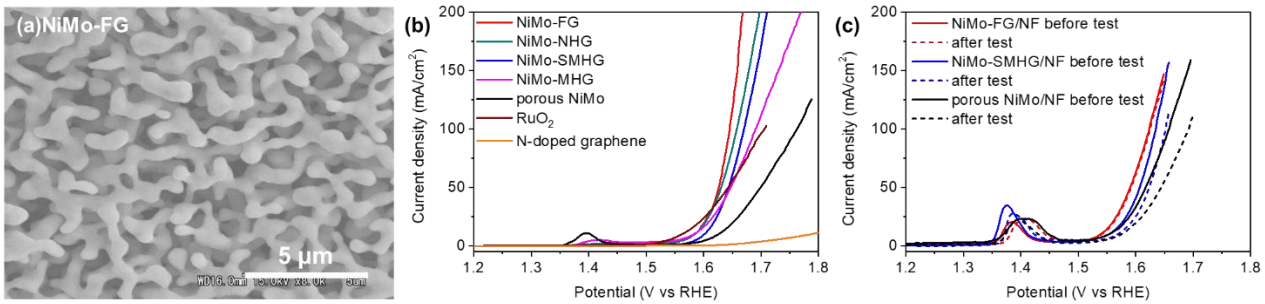

Figure 4 (a) The SEM image of NiMo-FG. (b) Hydrodynamic voltammograms of NiMo anodes with and without graphene encapsulation. (c) Cyclic voltammograms of various NiMo anodes deposited on Ni foam before and after 1000 cycles.

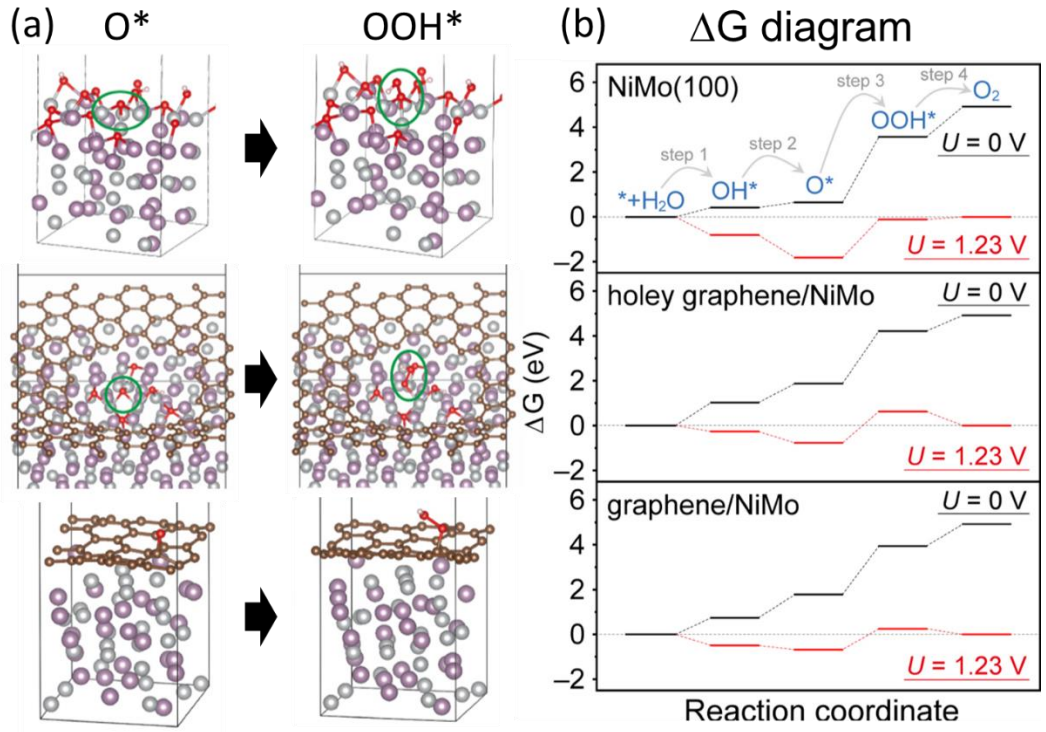

Figure 5 (a) Adsorption structures of intermediates and (b) DFT calculated Gibbs free energies during the OER processes on NiMo(100), holey graphene/NiMo, and graphene/NiMo. Steps 1, 2, 3, and 4 correspond to the chemical reactions.

3.3 Characterizations and evaluation of areal proton conductivity and crossover on the graphene membrane

In order to understand the proton permeation behaviors and formic acid crossover through graphene layers were systematically investigated under 0.05 M H_2SO_4 solution. The schematic diagram of the experiment concept is shown in **Figure 6a**. Electrochemical tests were performed on Nafion/Graphene/Nafion membranes, which are graphene-based materials reinforced with Nafion.

The areal proton conductivity through pure/defect graphene membranes with varied layer numbers, i.e., 1, 2, and 3-layers, was investigated by measuring the current-voltage (*I*-V) characteristic via the device (**Figure 6b**). The bias voltage, ranging from +200 mV to −200 mV, is applied between two Pt wire electrodes in a two-electrode system, the detected proton current varies linearly with bias voltages. The decreasing proton current was observed with the increasing number of graphene layers. It was observed that the areal proton conductivity decreased as the number of graphene layers increased, while the conductivity increased as more defects were introduced. The areal proton conductivity of a single layer of pure graphene (i.e., 1LG) was 0.06 mS/cm^2, while that of graphene with intentionally created nano-sized holes (defects) increased to 12.83 mS/cm^2. This conductivity is comparable to that of Nafion, which is commercially available.

Next, the formic acid crossover was evaluated. Thirty percent formic acid was added to the cathode chamber, and chronoamperometry (CA) measurements were performed at 1.6V. After the test, the electrolyte on the anode side was collected, and the amount of formic acid was quantitatively analyzed to estimate the crossover amount of formic acid. Compared to the case of Nafion alone, the crossover was successfully suppressed to less than half by sandwiching graphene-based material.

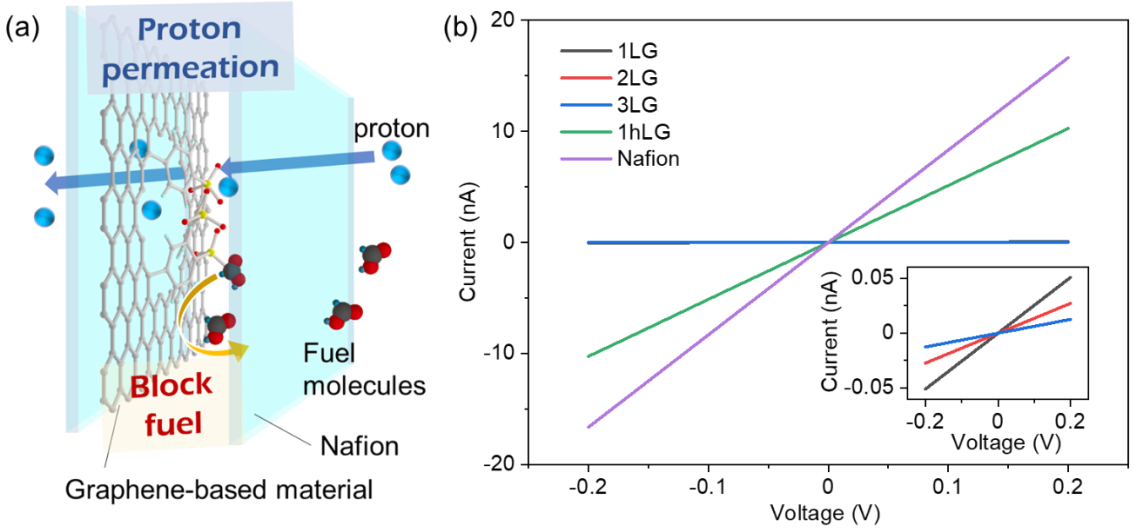

Figure 6 (a) Schematic diagram of the proton exchange membrane used in the experiment. The graphene-based material is sandwiched by the Nafion layer. (b) IV curve of membrane samples. 1,2 and 3LG refer to pure graphene with 1, 2, or 3 layers, respectively, and 1hG refers to graphene with nano-sized holes (defects).

4. Conclusions

In this study, elemental studies on cathode/anode catalysts and proton exchange membranes were carried out for the development of formic acid electrosynthesis cells by CO_2 electrochemical reduction. For the cathode electrocatalyst, the porous Sn catalyst was covered by PEG to improve mass transport to the catalyst surface, resulting in high formic acid selectivity and accelerating the formation rate of formic acid. The experimental results and DFT calculations showed that a proper PEG layer thickness facilitated the transport of CO_2 from the electrolyte to the catalyst surface. For the anode electrocatalyst, an OER catalyst with improved catalytic activity and durability was developed by graphene encapsulating on NiMo alloy. Such graphene encapsulation benefits the bifunctionality of electrochemically active sites and prevents the degradation of non-noble metal electrodes, thus realizing high catalytic performances and long lifetimes. Then, a novel proton exchange membrane with high proton conductivity and suppression of fuel molecule crossover was developed using graphene. It was achieved by creating appropriate lattice defects in graphene to increase the proton conductivity and by controlling the number of graphene layers to prevent the passage of fuel molecules. These developments on electrocatalysts and crossover suppression membranes are expected to significantly contribute to the realization of electrolytic cells, which are expected to be a technology for CO_2 utilization by CO_2ER.

5. References

1. Jothi, P. R.; Kannan, S.; Velayutham, G., Enhanced methanol electro-oxidation over in-situ carbon and graphene supported one dimensional $NiMoO_4$ nanorods. *Journal of Power Sources* **2015,** *277*, 350.

2. Fang, M.; Gao, W.; Dong, G. F.; Xia, Z. M.; Yip, S.; Qin, Y. B.; Qu, Y. Q.; Ho, J. C., Hierarchical NiMo-based 3D electrocatalysts for highly-efficient hydrogen evolution in alkaline conditions. *Nano Energy* **2016,**

3. Hu, K. L.; Jeong, S.; Wakisaka, M.; Fujita, J.; Ito, Y., Bottom-up Synthesis of Porous NiMo Alloy for Hydrogen Evolution Reaction. *Metals* **2018,** *8*, 9.

4. Ma, W. C.; Xie, S. J.; Zhang, X. G.; Sun, F. F.; Kang, J. C.; Jiang, Z.; Zhang, Q. H.; Wu, D. Y.; Wang, Y., Promoting electrocatalytic CO_2 reduction to formate via sulfur-boosting water activation on indium surfaces. *Nat. Commun.* **2019,** *10*, 10.

5. Ringe, S.; Clark, E. L.; Resasco, J.; Walton, A.; Seger, B.; Bell, A. T.; Chan, K., Understanding cation effects in electrochemical CO_2 reduction. *Energy Environ. Sci.* **2019,** *12* (10), 3001-3014.

6. Liu, M.; Pang, Y. J.; Zhang, B.; De Luna, P.; Voznyy, O.; Xu, J. X.; Zheng, X. L.; Dinh, C. T.; Fan, F. J.; Cao, C. H.; de Arquer, F. P. G.; Safaei, T. S.; Mepham, A.; Klinkova, A.; Kumacheva, E.; Filleter, T.; Sinton, D.; Kelley, S. O.; Sargent, E. H., Enhanced electrocatalytic CO_2 reduction via field-induced reagent concentration. *Nature* **2016,** *537*, 382.

7. Verma, S.; Lu, X.; Ma, S. C.; Masel, R. I.; Kenis, P. J. A., The effect of electrolyte composition on the electroreduction of CO_2 to CO on Ag based gas diffusion electrodes. *Phys. Chem. Chem. Phys.* **2016,** *18*, 7075.

List of Publications and Presentations

A) Publications

[1] **Samuel Jeong**, Tatsuhiko Ohto, Tomohiko Nishiuchi, Yuki Nagata, Jun-ichi Fujita, and Yoshikazu Ito, "Polyethylene Glycol Covered Sn Catalysts Accelerate the Formation Rate of Formate by Carbon Dioxide

Reduction", *ACS Catal.*, 2021, 11, 9962

[2] **Samuel Jeong**, Kailong Hu, Tatsuhiko Ohto, Yuki Nagata, Hideki Masuda, Jun-ichi Fujita, Yoshikazu Ito, "Effect of Graphene Encapsulation of NiMo Alloys on Oxygen Evolution Reaction", *ACS Catal.*, 2020, 10, 792.

[3] **Samuel Jeong**, Gary Edwards, Yoshikazu Ito, Jun-ichi Fujita, "High-sensitivity visualization of localized electric fields using low-energy electron beam deflection", *Jpn. J. Appl. Phys*. 2018, 57, 065201.

[4] Stefano Lupi, Luca Tomarchio, Salvatore Macis, Annalisa D'Arco, Antonio Grilli, Martina Romani, Mariangela Cestelli Guidi, Kailong Hu, Suresh Kukunuri, **Samuel Jeong**, Augusto Marcelli, Yoshikazu Ito, and Sen Mou, "Disordered Photonics Behavior from Terahertz to Ultraviolet of a 3-Dimensional Graphene Network", *NPG Asia Materials*, 2021, 13, 73.

[5] Aimi Asilah Haji Tajuddin, Ganesan Elumalai, Zeyu Xi, Kailong Hu, **Samuel Jeong**, Kensaku Nagasawa, Jun-ichi Fujita, Yoshitsugu Sone, and Yoshikazu Ito, "Corrosion-resistant Non-noble Metal Electrodes for PEM-type Water Electrolyzer", *Int. J. Hydrogen Energy*, 2021, 46, 38603.

[6] Yoshikazu Ito, Suresh Kukunuri, **Samuel Jeong**, Ganesan Elumalai, Aimi Asilah Haji Tajuddin, Zeyu Xi, Kailong Hu, and Tatsuhiko Ohto, "Phase-Dependent Electrochemical CO_2 Reduction Ability of NiSn Alloys for Formate Generation", *ACS Appl. Energy Mater.* 2021, 4, 7122.

[7] Takuya Tsujiguchi, Yusuke Kawabe, **Samuel Jeong**, Tatsuhiko Ohto, Suresh Kukunuri, Hirotaka Kuramochi, Yasufumi Takahashi, Tomohiko Nishiuchi, Hideki Masuda, Mitsuru Wakisaka, Kailong Hu, Ganesan Elumalai, Jun-ichi Fujita, Yoshikazu Ito, "Acceleration of Electrochemical CO_2 Reduction to Formate at the Sn/Reduced Graphene Oxide Interface", *ACS Catal.*, 2021, 11, 3310.

[8] Kailong Hu, **Samuel Jeong**, Ganesan Elumalai, Suresh Kukunuri, Jun-ichi Fujita, and Yoshikazu Ito, "Phase-Dependent Reactivity of Nickel Molybdates for Electrocatalytic Urea Oxidation," *ACS Appl. Energy Mater.*, 2020, 3, 7535.

[9] Akichika Kumatani, Chiho Miura, Hirotaka Kuramochi, Tatsuhiko Ohto, Mitsuru Wakisaka, Yuki Nagata, Hiroki Ida, Yasufumi Takahashi, Kailong Hu, **Samuel Jeong**, Jun-ichi Fujita, Tomokazu Matsue, Yoshikazu Ito, "Chemical Dopants on Edge of Holey Graphene Accelerate Electrochemical Hydrogen Evolution Reaction", *Adv. Sci.* 2019, 1900119.

[10] Kailong Hu, **Samuel Jeong**, Mitsuru Wakisaka, Jun-ichi Fujita, Yoshikazu Ito, "Bottom-Up Synthesis of Porous NiMo Alloy for Hydrogen Evolution Reaction", *Metals.* 2018, 8, 83.

B) Presentations

[11] **Samuel Jeong**, Kailong Hu, Tatsuhiko Ohto, Yuki Nagata, Hideki Masuda, Jun-ichi Fujita, and Yoshikazu Ito, "Graphene Encapsulation Effects on NiMo Alloy in Oxygen Evolution Reaction", MATERIALS RESEARCH MEETING 2019 (MRM2019), Yokohama, Kanagawa, Japan, December 12, 2019 (poster)

[12] **Samuel Jeong**, Gary Edwards, and Jun-ichi Fujita, "High sensitive visualization of localized electric field using low energy electron beam deflection", THE 61ST INTERNATIONAL CONFERENCE ON ELECTRON, ION, AND PHOTON BEAM TECHNOLOGY AND NANOFABRICATIONEIPBN 2017 (EIPBN2017), Orlando, Florida, US, May 30-June 2, 2017 (Oral)